Editors' Suggestion

Generation of High-Power High-Intensity Short X-Ray Free-Electron-Laser Pulses

Marc W. Guetg,* Alberto A. Lutman, Yuantao Ding, Timothy J. Maxwell, Franz-Josef Decker, Uwe Bergmann, and Zhirong Huang
SLAC National Accelerator Laboratory, Menlo Park, California 94025, USA

(Received 14 July 2017; published 3 January 2018)

X-ray free-electron lasers combine a high pulse power, short pulse length, narrow bandwidth, and high degree of transverse coherence. Any increase in the photon pulse power, while shortening the pulse length, will further push the frontier on several key x-ray free-electron laser applications including single-molecule imaging and novel nonlinear x-ray methods. This Letter shows experimental results at the Linac Coherent Light Source raising its maximum power to more than 300% of the current limit while reducing the photon pulse length to 10 fs. This was achieved by minimizing residual transverse-longitudinal centroid beam offsets and beam yaw and by correcting the dispersion when operating over 6 kA peak current with a longitudinally shaped beam.

DOI: 10.1103/PhysRevLett.120.014801

The x-ray free-electron lasers (XFELs) are the brightest x-ray light sources for scientific applications [1–4], having a peak brightness of about 9 orders of magnitude higher than storage-ring synchrotron sources. XFEL pulses are also characterized by ultrashort pulse durations, from a few to hundreds of femtoseconds, and are almost fully transverse coherent. Those unique features are used in a broad field of scientific investigation, including atomic, molecular, and optical physics, condensed matter physics, matter in extreme conditions, materials science, chemistry, and biology [5,6]. Single-particle imaging [7,8], for example, requires intense photon pulses to avoid structural modifications during the probe pulse duration (probe before destroy). In order to obtain subnanometer resolution, x-ray pulses that are shorter than 10 fs are required [9]. Similarly, serial femtosecond x-ray crystallography and x-ray spectroscopy studies would benefit from brighter and shorter x-ray pulses exploiting this same principle [10,11]. XFELs have also revealed a variety of nonlinear phenomena when intense x-ray pulses interact with atoms and molecules [12–14], including stimulated x-ray emission [15–17]. For the study of such nonlinear effects and their ultrafast dynamics, more intense and shorter pulses are needed. In fact, these novel methods such as stimulated x-ray emission are critically dependent on the maximum achievable peak intensity at short pulse lengths. Here a factor of 3 increase in the incident peak intensity can lead to a signal increase by 4 orders of magnitude [15–17]. As these experiments are currently at the borderline of feasibility and limited to demonstrations on model systems, more peak intensity is needed to advance the field of nonlinear x-ray science. Therefore, the method presented here is an important step in pushing several frontiers of XFEL science. Unfortunately, improvement in the XFEL power is very challenging. At present, the highest peak power is ~100 GW with a horn-collimation technique at the Linac Coherent Light Source (LCLS) [18]. Schemes demonstrated to manipulate the pulse duration down to a few femtoseconds have not increased the FEL power [19–21].

In a FEL, the achievable power at saturation scales with the electron bunch current as $P_{\mathrm{sat}} \propto I^{4/3}$ [22] and also when a postsaturation taper is usually applied to extract more power [23]. Therefore, an increase in the current leads to a higher saturation power. However, increasing the electron bunch current is not trivial, being limited mainly by microbunching instabilities and coherent synchrotron radiation (CSR). Microbunching instabilities are strongly reduced by laser heating prior to bunch compression, at the cost of an increase of the uncorrelated energy spread [24]. CSR leads to a longitudinally dependent energy loss along the bunch. The subsequent bends translate this energy difference to a transverse misalignment of the longitudinal slices of the bunch, expressed by the beam yaw. So far, the beam yaw introduced at higher compressions has prevented the use of very high current bunches in the production of x-rays. Yawed beams affect the XFEL performance negatively because of nonuniform lasing. This leads to a lower number of photons per pulse and a more difficult FEL optimization process. Beam yaws are mitigated by proper beam optics [25] but cannot be fully reverted. A recent paper based on theory and simulations proposed a method to remove the beam yaw [26,27] by the careful control of dispersion at locations with a strong energy chirp (e.g., the bunch compressors) by multipole magnets. The energy chirp thereby links the dispersion with the beam yaw, which in turn allows the beam yaw manipulation through dispersion. Assuming a linear energy chirp, the beam yaw can be influenced linearly by the quadrupole tweaker magnet and quadratically by sextupole tweaker magnets. Foundations for higher order are given in Ref. [26]. The described correction is a trade-off between

the residual lattice dispersion and beam yaw, as previously both could not be corrected simultaneously. This theory of linear correction was demonstrated at a low-energy electron beam [26].

Following the same approach and definitions introduced in this theoretical work, we discriminate between lattice and electron bunch dispersion. The lattice dispersion $\hat{\eta}$ between two locations in the machine describes the relation between the incoming energy and the outgoing transverse displacement in the position and angle. Lattice dispersion does not depend on the initial condition of the beam but only on the transport lattice. Some machine sections like the two bunch compressors (BCs) or the dogleg (see Fig. 1) are designed to present a lattice dispersion. Common sources of lattice dispersion are quadrupole offsets and dipole orbit correctors. The lattice dispersion is measured by the electron bunch trajectory as a function of the beam energy. The beam energy can be varied by modifying a phase of an accelerating cavity. Parasitic measurements are possible if the electron shot-to-shot energy jitter is sufficient. The beam yaw μ is a correlation between the longitudinal and transverse positions of the charged particles within the bunch. The beam yaw μ is only related to the phase space charge distribution and does not carry information about its origin. Three common sources of beam yaw are lattice dispersion in combination with an energy chirp, transverse wakefields, and CSR. The beam yaw can be measured destructively by streaking the electron bunch onto a screen. Streaking is provided by time-dependent fields like the ones produced in transverse deflecting cavities or in wakefield-based passive streakers [28,29]. Bunch dispersion η defines the correlation between the energy and transverse position within the bunch. In first order, it correlates with the beam yaw by $\mu \approx \eta\alpha_z/\beta_z$ in the presence of a strong energy chirp ($|\alpha_z| \gg 0$) [26], where α_z and β_z correspond to the longitudinal Twiss parameters. The bunch dispersion is measured similarly to the beam yaw, by streaking in momentum instead of longitudinal position. A change in the lattice dispersion results in the same change in beam dispersion but not vice versa. All the introduced properties are defined in both the transverse momentum and position.

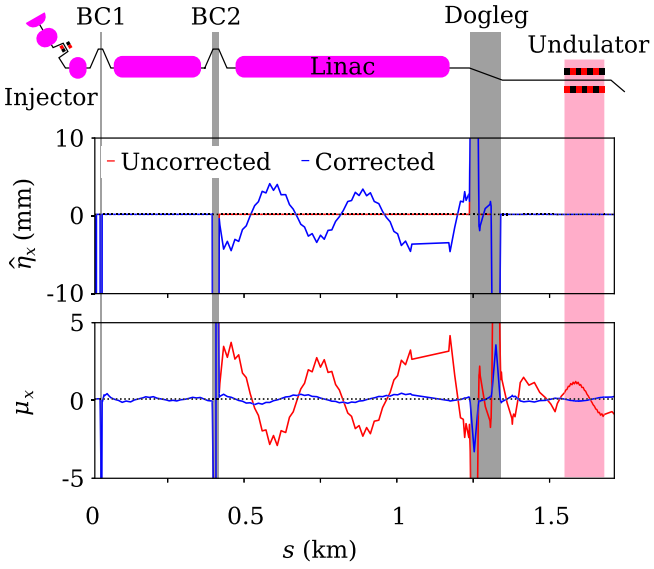

FIG. 1. ELEGANT [30] simulation of the LCLS showing beam yaw (μ) and lattice ($\hat{\eta}$) dispersion prior and after a beam yaw correction. Included sources of beam yaw are the transverse wakefields and the CSR. The correction was done using a singular value decomposition algorithm as further detailed in Ref. [26]. The dispersive areas housing the tweaker quadrupole magnets are highlighted in gray. Note that leaked lattice dispersion is increased between BC2 and the dogleg; measurements at LCLS agree with both the phase and magnitude of this intermediate increase.

The correction of both the beam yaw and lattice dispersion allows one to operate with stronger longitudinal compression, without suffering performance degradation due to the beam yaw. Therefore, this scheme allows a higher operational current resulting not only in shorter photon pulses but also an increased FEL parameter ($\rho \propto \text{current}^{4/3}$) [22], which in turn is proportional to the FEL power. The simultaneous reduction of lattice dispersion removes the electron energy orbit correlation and in extension the photon power electron energy dependency, making the FEL power more stable.

The strength of the tweaker quadrupole magnet within a dispersive section controls the lattice dispersion in momentum ($\hat{\eta}'$). A correction in the momentum and position requires a minimum of two tweaker quadrupole magnets separated by a phase advance different than a multiple of π [ideally by $\pi(n+\frac{1}{2})\colon n \in \mathbb{N}_0$]. Manipulation of the beam yaw follows through changing the bunch dispersion, thereby requiring an energy chirp. As for the lattice dispersion, the correction of the beam yaw in momentum and position requires two quadrupole magnets. Correction of both the beam yaw and lattice dispersion therefore requires at least two pairs of tweaker quadrupole magnets (four in total) at locations where the bunch has different energy chirps and adequate phase advance between the pairs. In theory, the phase advance between the tweaker quadrupole magnet pairs does not influence the possibility of the correction.

The LCLS is equipped with a total of six tweaker quadrupole magnets for dispersion control, a pair in each bunch compressor and one pair in the final dogleg. The combination of the BC2 and dogleg quadrupole tweakers is linearly independent and is therefore sufficient for correction. Figure 1 shows an ELEGANT [30] optimization for a typical correction case using the pair of BC2 and dogleg quadrupole magnet tweakers.

Initial experiments of beam yaw correction were previously performed [31] for operation in the overcompression mode. Overcompressing the electron bunch in the

TABLE I. Operational parameters during a user run implementing the proposed method. The sample size is 1190 shots.

Parameter	Mean	rms	Typical values[a]
Charge at the gun (pC)	250	2	250
Charge at the undulator (pC)	128	1	180
BC1 peak current (A)	160	3	220
BC2 peak current (A)	6000	330	3500
Electron Energy (MeV)	12 000	6	12 000
Photon peak power (GW)	276	26	90
Photon pulse energy (mJ)	3.4	0.34	3500
Photon pulse FWHM (fs)	10.3	1.6	11

[a]Typical values are taken from recent runs at similar conditions with an emittance spoiler [32].

second bunch compressor flips the sign of the energy chirp. The longitudinal wakefields are now additive, resulting in an energy chirp at the percent level. This energy chirp allowed one to streak the beam by dispersion and measure the beam yaw. In contrast, this Letter concentrates on the undercompression operating point. During undercompression operation, the energy chirp required for compression is removed by the longitudinal wakefields in the third linac section. The undercompression mode provides a narrower FEL bandwidth and is therefore preferred by most LCLS users. The absence of an energy chirp at the end on the machine in the undercompression mode does not allow a dispersion-based diagnostic of the beam yaw.

The scheme was experimentally demonstrated at the LCLS operating in a high-current mode at a photon energy of 6.6 keV, with an electron beam energy of 12 GeV. A standard operating point at this energy is ~3 kA. To reach a higher current, stronger compression in the second bunch compressor was adopted. The nonlinearities, such as the beam third-order time-energy curvature induced from the wakefield in the linac structures and the high-order optics terms in the compression chicanes, will lead to a current spike in the head and tail of the compressed bunch. This nonuniform current distribution causes stronger collective effects such as from CSR, space charge force, and downstream wakefields, which degrade the FEL performance. Recently, a beam-shaping method by collimating the bunch head and tail at the first bunch compressor has been applied to counteract these effects [18]. Starting from an electron bunch charge of 250 pC in the gun, it is collimated to ~180 pC at regular operation, which improves the current distribution and the FEL performance. In this study, using a higher current we truncated more on the bunch head and tail with about half of the charge left. This achieved a better time-energy linearity on the beam as well as limiting higher-order beam yaws. We measured a current of 6.3 kA in the second bunch compressor, well above the standard operating point at this energy of 3 kA. Then we applied the yaw and dispersion correction as discussed in the following for high FEL power operation. Table I summarizes the electron bunch conditions.

Figure 2 shows the experimentally measured effect of the first tweaker quadrupole in BC2 on various photon and electron beam properties. The scan of one tweaker quad shows its effect on both lattice dispersion and beam yaw. Figure 2(a) shows the FEL pulse energy as a function of the tweaker quadrupole magnet strength. The pulse energy has a bell-like shape, clearly identifying a maximum, corresponding close to but not at the minimum of the lattice dispersion [see Fig. 2(c)]. The pulse energy decays quickly as the dispersion grows bigger. Figure 2(b) shows the average spectrum for photon pulses produced by electron bunches with energies between 11 998 and 12 002 MeV. Such pulse filtering is required to show the effect of the tweaker quadrupole magnet on the pulse spectrum avoiding contamination due to the correlation between the radiation wavelength and electron beam energy. Since the electron

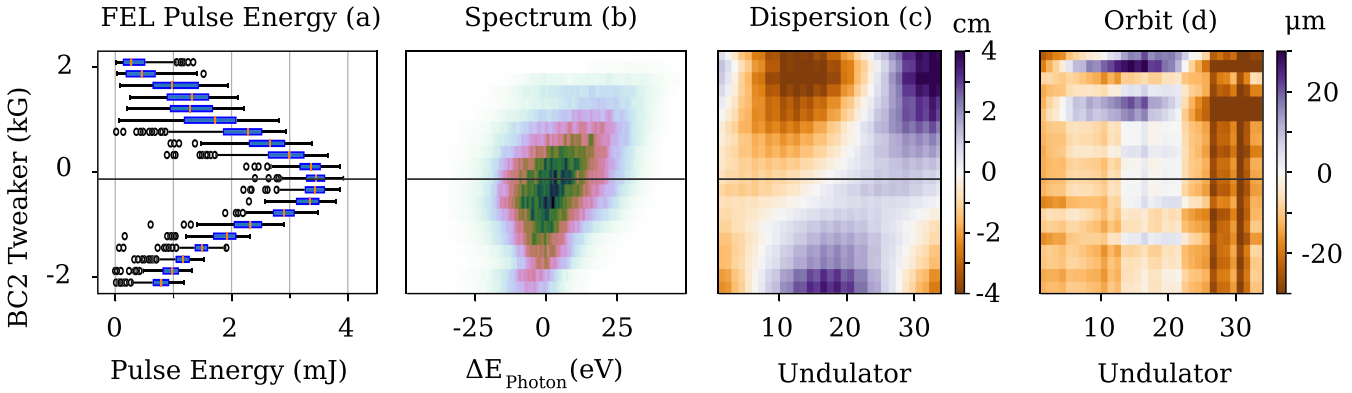

FIG. 2. Effects of a tweaker quadrupole magnet in BC2. FEL pulse energy, pulse energy measured by the gas detector; spectrum, average photon spectrum of electron energy 12 000 ± 2 MeV; dispersion, lattice dispersion within the undulator measured by beam position monitor correlation; orbit, average orbit within the undulator. All data originate from one scan recorded beam synchronously. Beam parameters: charge, 150 pC; peak current, 7 kA; electron energy, 12 GeV and a small energy chirp; photon energy, 6.6 keV. The black line denotes the optimal performance.

bunch at the undulator has a residual energy chirp, the spectrum resembles the lasing along the bunch. Therefore, a selective lasing at a bunch end for the lower values of the quadrupole tweaker magnet followed by uniform lasing along the core of the bunch and then selective lasing at the other bunch end is observed [Fig. 2(b)]. This phenomenon has been described in more detail in both a theory [26] and an experiment [33]. Longitudinal effects due to the additional nonlinear compression terms are minimal as shown by both simulations and measurements by the transverse deflector [34]. The lattice dispersion within the undulator depends also on the strength of the scan magnet. The minimum lattice dispersion is shifted with respect to the maximal lasing performance. This proves that the lasing performance depends on both the lattice dispersion and beam yaw, and minimization of the lattice dispersion alone does not guarantee optimal performance. With the proposed scheme, it is possible to minimize both the lattice dispersion and beam yaw. The dispersion measurement furthermore outlines a phase advance of somewhat less than 2π along the undulator, which agrees well with the design optics. The measured dispersion is a superposition between the residual lattice dispersion and the dispersion generated by the scanning tweaker quadrupole. A second corrector with a nonmultiple of π phase advance to the first one would be necessary to completely cancel the dispersion. The orbit measurements confirm that the lasing was not suppressed by a center of mass offset within the undulator, as the orbits measured in Fig. 2(d) do not justify the lasing suppression shown in Fig. 2(a).

Table I shows the measured performance parameters using the proposed correction scheme. The peak current is a compromise between power and stability. The strong compression increases the sensitivity of peak current to rf timing jitter. The power jitter (9.4%) is dominated by the peak current (7.3% contribution). Newer accelerators, specifically but not limited to ones driven by superconducting rf and solid state amplifiers, with better rf phase stability will allow for more stable compression [35–39].

Compression nonlinearities, not removed by the higher harmonic acceleration cavity, lead to current spikes at the beginning and the end of the electron beam. These current spikes greatly enhance CSR and other collective effects such as space charge, both of which reduce FEL performance. The longitudinal phase space within BC1 is ordinarily collimated to counteract this effect [18]. The stronger compression requires an additional 25% of truncation. The reduced charge had the additional upside of shorter bunches at similar final peak currents.

Figure 3 shows the temporal reconstruction of two typical shots. The top shows the longitudinal phase space of the electrons after the undulator. The FEL process leads to an energy loss of individual particles and a slice energy spread increase. Both of these processes allow a temporal reconstruction of the x-ray pulse [34]. The measurements

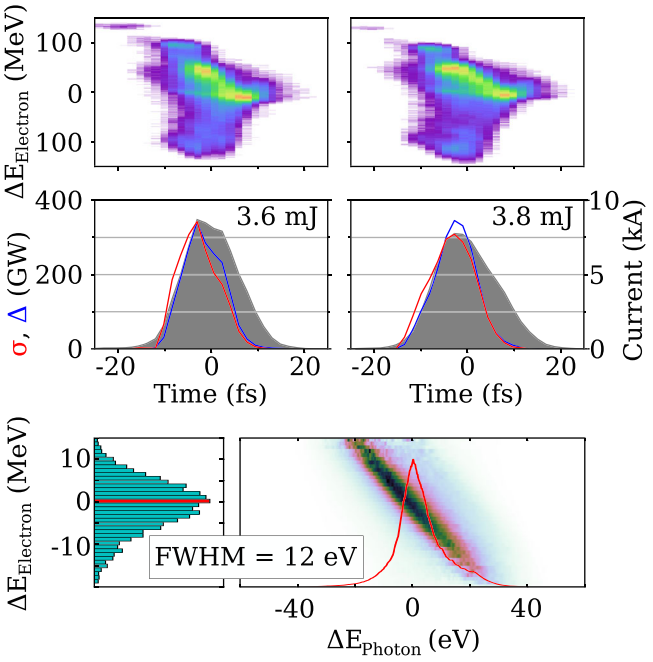

FIG. 3. Top: Longitudinal electron phase space after the undulator. Middle: Photon power calculated by energy loss (Δ, red curve), slice energy spread (σ, blue curve) [34], and current profile (gray). Bottom: Average photon spectra sorted by electron energy. Bunch charge, 140 pC; electron energy, 12 GeV; photon energy, 6.6 keV.

show a fractional energy loss of up to 1.2% together with a uniform lasing along the bunch. Note that the perceived energy chirp originates from the undulator wakes. Deconvolution of it shows a complete absence of an energy chirp at the beginning of the undulator.

Because of the high current, the electron beam was truncated stronger than for normal operation. The missing initial current spike leads to reduced longitudinal wakefields required for the removal of the residual energy chirp. The diminution of the longitudinal wakefields was more than compensated for by the higher bunch current within the final linac, 540 m *S*-band linac. The residual energy chirp had to be reduced by lowering the BC1 compression factor while keeping the final peak current constant [18]. This leads to a stronger energy chirp entering the final linac canceling the longitudinal wake field of the third linac. Alternatively, the lattice compression factor (R_{56}) of BC2 could have been lowered, leading to the same effect.

Binning by the incoming electron beam energy and averaging leads to a final photon energy bandwidth of 0.18% at 6.6 keV. This low photon bandwidth further increases the brilliance, which is therefore worth its own pursuit, as it may allow the conduction of experiments normally requiring either seeding or a monochromatizer.

This Letter describes the experimental realization of correcting for CSR by minimizing both the beam yaw and lattice dispersion. While the beam yaw correction has been

previously described theoretically [26], we found that the large beam energy jitter inherent to LCLS required additional lattice dispersion. By combining the yaw correction with longitudinal beam shaping [18], we were able to increase the peak current above 6 kA. This corresponds to a more than 3 times higher FEL peak power for short bunch operation as compared to the previous maximum. In addition, the spectral brightness of the x-ray pulses was further increased by reducing the electron bandwidth. The maturity of this method is underlined by the fact that it has been already successfully implemented into LCLS operations. The combination of this technique with an emittance spoiler [32] allows for even shorter pulses. It is important to note that the peak current we achieved was mainly limited by rf stability; hence, further improvements are expected for the new, more stable FEL sources. Finally, simulation studies for LCLS and SwissFEL [26] showed that a second-order beam yaw correction can be achieved by the addition of sextuple magnets in dispersive sections. As for the linear correction, this would require four sextuple magnets for a theoretically perfect correction of both second-order beam yaw and chromaticity.

This work has been supported by DOE Contract No. DE-AC02-76SF00515. The authors thank Paul Emma, Gabriel Marcus, and Chao Yu-Chiu for fruitful discussions. Furthermore, the authors thank the operators of LCLS for their excellent handling of the machine.

*marcg@slac.stanford.edu

[1] P. Emma *et al.*, Nat. Photonics **4**, 641 (2010).
[2] T. Ishikawa *et al.*, Nat. Photonics **6**, 540 (2012).
[3] E. Allaria *et al.*, Nat. Photonics **7**, 913 (2013).
[4] W. Ackermann *et al.*, Nat. Photonics **1**, 336 (2007).
[5] C. Bostedt, S. Boutet, D. M. Fritz, Z. Huang, H. J. Lee, H. T. Lemke, A. Robert, W. F. Schlotter, J. J. Turner, and G. J. Williams, Rev. Mod. Phys. **88**, 015007 (2016).
[6] *X-Ray Free Electron Lasers*, edited by U. Bergmann, V. Yachandra, and J. Yano (Royal Society of Chemistry, London, 2017).
[7] M. M. Seibert *et al.*, Nature (London) **470**, 78 (2011).
[8] Aquila *et al.*, Struct. Dyn. **2**, 041701 (2015).
[9] A. Aquila (private communication).
[10] A. Barty *et al.*, Nat. Photonics **6**, 35 (2011).
[11] H. N. Chapman, C. Caleman, and N. Timneanu, Phil. Trans. R. Soc. B **369**, 20130313 (2014).
[12] Young *et al.*, Nature (London) **466**, 56 (2010).
[13] T. E. Glover *et al.*, Nature (London) **488**, 603 (2012).
[14] J. Stöhr and A. Scherz, Phys. Rev. Lett. **115**, 107402 (2015).
[15] N. Rohringer *et al.*, Nature (London) **481**, 488 (2012).
[16] C. Weninger, M. Purvis, D. Ryan, R. A. London, J. D. Bozek, C. Bostedt, A. Graf, G. Brown, J. J. Rocca, and N. Rohringer, Phys. Rev. Lett. **111**, 233902 (2013).
[17] H. Yoneda, Y. Inubushi, K. Nagamine, Y. Michine, H. Ohashi, H. Yumoto, K. Yamauchi, H. Mimura, H. Kitamura, T. Katayama, T. Ishikawa, and M. Yabashi, Nature (London) **524**, 446 (2015).
[18] Y. Ding *et al.*, Phys. Rev. Accel. Beams **19**, 100703 (2016).
[19] P. Emma, K. Bane, M. Cornacchia, Z. Huang, H. Schlarb, G. Stupakov, and D. Walz, Phys. Rev. Lett. **92**, 074801 (2004).
[20] Y. Ding *et al.*, Appl. Phys. Lett. **107**, 191104 (2015).
[21] A. A. Lutman, T. J. Maxwell, J. P. MacArthur, M. W. Guetg, N. Berrah, R. N. Coffee, Y. Ding, Z. Huang, A. Marinelli, S. Moeller, and J. C. U. Zemella, Nat. Photonics **10**, 745 (2016).
[22] P. Schmüser, M. Dohlus, and J. Rossbach, *Ultraviolet and Soft X-Ray Free-Electron Lasers: Introduction to Physical Principles, Experimental Results, Technological Challenges* (Springer Science, New York, 2008), Vol. 229.
[23] K.-J. Kim, Z. Huang, and R. Lindberg, *Synchrotron Radiation and Free-Electron Lasers: Principles of Coherent X-Ray Generation* (Cambridge University Press, Cambridge, England, 2017).
[24] Z. Huang *et al.*, Phys. Rev. ST Accel. Beams **13**, 020703 (2010).
[25] S. Di Mitri, M. Cornacchia, and S. Spampinati, Phys. Rev. Lett. **110**, 014801 (2013).
[26] M. W. Guetg, B. Beutner, E. Prat, and S. Reiche, Phys. Rev. ST Accel. Beams **18**, 030701 (2015).
[27] M. W. Guetg, Ph. D. thesis, ETH Zurich, 2015.
[28] K. Bane, G. Stupakov, and I. Zagorodnov, Report No. SLAC-PUB-16497, 2016.
[29] A. Novokhatski *et al.*, in *Proceedings of the Seventh International Particle Accelerator Conference (IPAC'16), Busan, Korea, 2016* (JACoW, Geneva, 2016), pp. 817–819.
[30] M. Borland, technical report, Argonne National Lab, 2000).
[31] M. Guetg, F.-J. Decker, Y. Ding, P. Emma, Z. Huang, and T. Maxwell, in *Proceedings of the Seventh International Particle Accelerator Conference (IPAC'16), Busan, Korea, 2016* (JACoW, Geneva, 2016), pp. 813–816.
[32] A. A. Lutman, R. Coffee, Y. Ding, Z. Huang, J. Krzywinski, T. Maxwell, M. Messerschmidt, and H.-D. Nuhn, Phys. Rev. Lett. **110**, 134801 (2013).
[33] M. W. Guetg, A. A. Lutman, Y. Ding, T. J. Maxwell, F.-J. Decker, A. J. Fisher, and Z. Huang (unpublished).
[34] C. Behrens *et al.*, Nat. Commun. **5**, 3762 (2014).
[35] LINAC Coherent Light Source II (LCLS-II), technical report, SLAC, 2015.
[36] W. Decking and T. Limberg, European XFEL GmbH, Hamburg, Germany, Report No. XFEL. EU TN-2013-004-01, 2013.
[37] *SwissFEL Conceptual Design Report*, edited by R. Ganter (PSI, Villigen, 2012).
[38] J. Han, in *Proceedings of the Seventh International Particle Accelerator Conference (IPAC'16), Busan, Korea, 2016* (JACoW, Geneva, 2016), pp. 6–10.
[39] Z. Huang and I. Lindau, Nat. Photonics **6**, 505 (2012).